Available online at www.sciencedirect.com
SCIENCE DIRECT
Chemical Physics Letters 427 (2006) 117–121
CHEMICAL PHYSICS LETTERS
www.elsevier.com/locate/cplett

D-band Raman intensity of graphitic materials as a function of laser energy and crystallite size

K. Sato [a,*], R. Saito [a,*], Y. Oyama [a], J. Jiang [a], L.G. Cançado [b], M.A. Pimenta [b], A. Jorio [b], Ge.G. Samsonidze [c], G. Dresselhaus [d], M.S. Dresselhaus [c,e]

[a] Department of Physics, Tohoku University and CREST, Sendai 980-8578, Japan
[b] Departamento de Física, Universidade Federal de Minas Gerais, Belo Horizonte-MG 30123-970, Brazil
[c] Department of Electrical Engineering and Computer Science, Massachusetts Institute of Technology, Cambridge, MA 02139-4307, USA
[d] Francis Bitter Magnet Laboratory, Massachusetts Institute of Technology, Cambridge, MA 02139-4307, USA
[e] Department of Physics, Massachusetts Institute of Technology, Cambridge, MA 02139-4307, USA

Received 11 April 2006; in final form 30 May 2006
Available online 6 June 2006

Abstract

The Raman intensity of the disorder-induced D-band in graphitic materials is calculated as a function of the in-plane size of the graphite nanoparticles (L_a) and as a function of the excitation laser energy. Matrix elements associated with the double resonance Raman processes, i.e., electron–photon, electron–phonon and electron–defect processes are calculated based on the tight binding method. The electron–defect interaction is calculated by considering the elastic scattering at the armchair edge of graphite, adopting a nanographite flake whose width is L_a. We compare the calculated results with the experimental results obtained from the spectra for different laser lines and L_a.

1. Introduction

Graphitic materials with many different types of translational breaking symmetry perturbations, such as nanometric-size crystallites, impurities, imperfections, edges, exhibit a Raman band in the range of 1200–1400 cm^{-1}, which is not present in the Raman spectrum of single-crystal graphite [1]. This disorder-induced band, usually called the D-band, has been used for many years to estimate the graphitic in-plane crystallite size L_a in disordered carbon materials, since the integrated intensity ratio I_D/I_G (the D-band integrated intensity divided by the integrated intensity of the Raman-allowed G-band) is proportional to L_a^{-1} [1].

Vidano et al. [2] performed a systematic investigation of the Raman spectra of different kinds of carbon materials by changing the laser excitation energy (E_{laser}) and they observed that the frequency of the D-band strongly depends on E_{laser}. The D-band frequency upshifts linearly with increasing E_{laser} over a wide laser energy range, the slope of this dependence being $\partial\omega_D/\partial E_{laser} \simeq 50\ cm^{-1}/eV$. After this work, the laser energy dependence of the D-band frequency was observed in many different graphitic materials, and the slope of this dependence was observed to be independent of the material type [3].

Mernagh et al. [4] have investigated the Raman spectrum of carbon black, and found that I_D/I_G of the bands at 1360 (D) and 1580 cm^{-1} (G) also depends on the laser energy E_{laser} used for the Raman excitation. This strong dependence of the ratio I_D/I_G on E_{laser} has been further observed in many different graphitic materials, as a-C materials [5], pyrolytic graphites [6], carbon nanotubes [7], disordered graphite [8] and in graphite edges [9] and in carbon foams [10]. Pócsik et al. showed the Raman spectra of a disordered graphite excited with several laser lines in the broad range between 1.16 and 4.13 eV, where both the E_{laser} dependences of the D-band frequency and the ratio I_D/I_G can be clearly observed [8].

* Corresponding author. Fax: +81 22 795 6447.
E-mail addresses: kentaro@flex.phys.tohoku.ac.jp (K. Sato), rsaito@flex.phys.tohoku.ac.jp (R. Saito).
URL: http://flex.phys.tohoku.ac.jp/ (R. Saito).

0009-2614/$ - see front matter © 2006 Elsevier B.V. All rights reserved.
doi:10.1016/j.cplett.2006.05.107

The first attempt to explain the dispersive behavior in the frequency of the D-band was presented by Baranov et al. [11], who proposed that this band originates from a double resonance (DR) Raman process in graphite. This concept was further developed by Thomsen and Reich [12] who calculated the scattering cross section for the double resonance mechanism that gives rise to the D-band. Saito et al. [13] generalized the concept of the D-band double resonance mechanism in graphite, and showed that it can be used to probe all phonon branches of graphite near the Γ and K points of the graphite two-dimensional (2D) Brillouin zone. It was also pointed out in this work [13] that the wavevectors q of the phonons associated with the D-band (measured from the K point) would couple preferentially with the electronic states with wavevectors k (measured from the K point) such that $q = 2k$. Moreover, it was shown that the D-band originates from an intervalley DR process, involving electronic states around two inequivalent K and K' points in the Brillouin zone of graphite, whereas the D*-band, which appears in the Raman spectrum around 1620 cm^{-1}, originates from an intravalley DR process involving electronic states around the same K point [13].

Despite the fact that the dispersive behavior of the D-band frequency has been successfully understood by the DR mechanism, the strong E_{laser} dependence of the ratio I_D/I_G is still an open problem. On the other hand, there is no theory that explains the dependence of ratio I_D/I_G on the crystallite size L_a. The complete understanding of the intensity of the D-band in graphitic materials as a function of E_{laser} and L_a is of fundamental importance since the intensity of the D-band has been commonly used for practical applications to evaluate the amount of disorder in carbon materials. The purpose of this work is to explain the dependence of the ratio I_D/I_G both on the crystallite size L_a and on the laser energy E_{laser}.

In Section 2 we present the experimental results about E_{laser} and L_a dependence of the ratio I_D/I_G. In Section 3 we explain how to calculate and observe the D-band intensity. In Section 4 we compare calculated results and corresponding experimental results. In Section 5 the summary is given.

2. Experimental results

The samples of disordered graphite used in this work are polyparaphenylene (PPP)-based carbon, heat-treated at different temperatures, and the crystallite sizes increases with increasing heat treatment temperatures. In a previous work, X-ray diffraction measurements have shown that the PPP samples heat-treated at 1500–2700 °C exhibit only an sp^2-carbon phase with poor graphitization behavior (stacking order along the c-axis) [14]. Therefore, the samples used in this work can be considered as a good prototype of 2D graphite. The Raman spectra were performed at room temperature, using a triple monochromator micro-Raman spectrometer (DILOR XY) for the following laser energies:

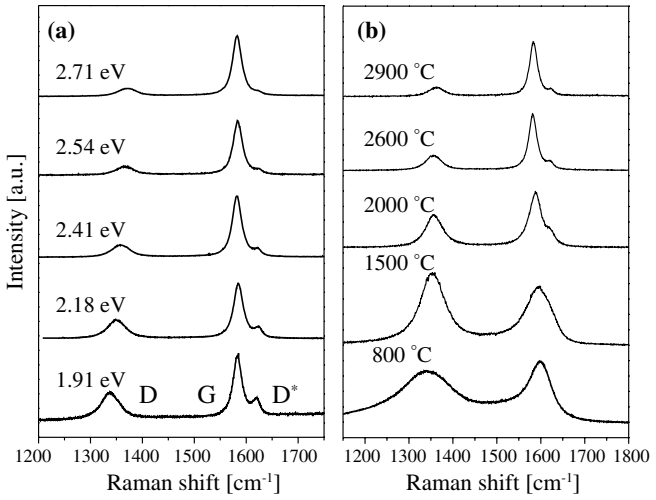

Fig. 1. The first order Raman spectra of (a) PPP-2900 with different laser energies, and (b) PPP samples with different heat treatment temperatures.

Krypton 1.91 and 2.18 eV, and Argon 2.41, 2.54 and 2.71 eV. The laser power density used here was always less than 10^5 W/cm^2.

Fig. 1(a) shows the first order Raman spectra of PPP sample heat-treated at 2900 °C (PPP-2900) using five different laser energies (1.91, 2.18, 2.41, 2.54, and 2.71 eV). The intensities were normalized so that the G-band has the same integrated intensity for all spectra. Note that both the D-band frequency and I_D/I_G ratio depend on the L_a used in the experiment. Fig. 1(b) shows the Raman spectra for PPP samples treated at different temperatures, between 1500 and 2900 °C, using 2.41 eV excitation laser energy. As will be discussed, the crystallite size of the graphite crystallites increases with increasing temperature [15]. Thus Fig. 1(b) shows that I_D/I_G decreases with increasing L_a. Note that I_D/I_G decreases significantly with increasing laser energy.

The L_a values of the different PPP samples are obtained indirectly from the values of the ratio I_D/I_G for the Raman spectra obtained using $E_{laser} = 2.41$ eV, by evaluating the relation L_a (Å) $= 5600\, E_{laser}^{-4}(I_D/I_G)^{-1}$ [15]. This relation is established recently in Ref. [15], where the authors compared the Raman data of disordered carbon films heat-treated at different temperatures with the respective L_a values obtained from STM images and very accurate X-ray diffraction data. Experimental results show a strong dependence of the D-band frequency on L_a. However in this paper, we do not consider this dependence since the frequency depends on the shape of the graphene flake and the corresponding resonance condition.

3. Calculation method

In order to calculate the dependence of the D-band intensity on the crystallite size L_a, we consider a graphite square flake with length L_a (see Fig. 2). All the integration on k is taken for discrete k values. The D-band intensity is

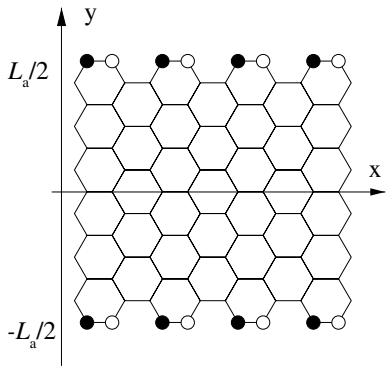

Fig. 2. The model of a nanographite flake with the armchair edge at $y = \pm L_a/2$ and a zigzag edge at $x = \pm L_a/2$.

calculated for a nanographite flake with an armchair edge [16]. The nanographite flake has an armchair edge at $y = \pm L_a/2$ and a zigzag edge at $x = \pm L_a/2$ as shown in Fig. 2 [17]. In a previous paper, we showed that the zigzag edge does not contribute to the elastic scattering from the K to K' points in the Brillouin zone [16]. Thus we make a simple model with the armchair edge in which we consider that the elastic scattering at the edge is expressed by the width of the nanographite flake L_a. In the real disordered graphite, we expect different kinds of defects. We select this model for getting an analytic expression of the elastic scattering.

The Raman intensity of the D-band, which is given by the double resonance scattering processes, is there [18],

$$I(\omega_{\mathrm{ph}}, E_{\mathrm{laser}}) = \sum_j \left| \sum_{a,b,c,\omega_{\mathrm{ph}}} \frac{M_{\mathrm{op}}(\boldsymbol{k}, jc) M_{\mathrm{elastic}}(-\boldsymbol{q}, cb) M_{\mathrm{ep}}(\boldsymbol{q}, ba) M_{\mathrm{op}}(\boldsymbol{k}, aj)}{\Delta E_{aj}(\Delta E_{bj} - \hbar\omega_{\mathrm{ph}})(\Delta E_{aj} - \hbar\omega_{\mathrm{ph}})} \right|^2, \tag{1}$$

where

$$\Delta E_{aj} = E_{\mathrm{laser}} - (E_a - E_j) - \mathrm{i}\gamma, \tag{2}$$

and γ denotes the broadening factor. In this calculation, we take $\gamma = 0.06$ eV [18]. Here j, a, b and c denote the initial states, the excited states, the first scattered state of an electron by a phonon and the second scattered state of an electron by a defect, respectively. M_{op}, M_{ep} and M_{elastic} denote the electron–photon, electron–phonon and elastic scattering matrix elements, respectively. Hereafter, we compare the calculated, integrated intensities I_D and I_G with experimental ones.

3.1. Elastic scattering

The elastic scattering at the armchair edges from $\boldsymbol{k}$ to $\boldsymbol{k}'$ is expressed by

$$M_{\boldsymbol{k}'\boldsymbol{k}} = \langle \Psi^{\mathrm{c}}(\boldsymbol{k}') | V | \Psi^{\mathrm{c}}(\boldsymbol{k}) \rangle, \tag{3}$$

in which $\Psi^{\mathrm{c}}(\boldsymbol{k})$ is the conduction-band wavefunction of 2D graphite at wavevector $\boldsymbol{k}$ and V is the potential term of the Hamiltonian. $\Psi(\boldsymbol{k})$ is expanded by the Bloch wavefunction Φ_s,

$$\Psi^{\mathrm{c}}(\boldsymbol{k}, \boldsymbol{r}) = \sum_{s=\mathrm{A,B}} C_s(\boldsymbol{k}) \Phi_s(\boldsymbol{k}, \boldsymbol{r}), \tag{4}$$

and Φ_s is expressed by the atomic wavefunction, $\varphi(r–\boldsymbol{R}_s)$

$$\Phi_s(\boldsymbol{k}, \boldsymbol{r}) = \frac{1}{\sqrt{N_{\mathrm{u}}}} \sum_{\boldsymbol{R}_s} e^{\mathrm{i}\boldsymbol{k}\cdot\boldsymbol{R}_s} \varphi(\boldsymbol{r} - \boldsymbol{R}_s), \tag{5}$$

in which N_{u}, $C(\boldsymbol{k})$, $\boldsymbol{R}_s$ are, respectively, the number of graphite unit cells in the flake, the wave function coefficients and the coordinates of the A and B atoms of the sth unit cell in the flake and appearing in the atomic orbital. In the absence of a defect, $\Phi(\boldsymbol{k})$ is the eigenfunction of 2D graphite. When we put Eq. 4 into Eq. 3, we get

$$M_{\boldsymbol{k}'\boldsymbol{k}} = \frac{1}{N_{\mathrm{u}}} \sum_{s,s'} C^*_{s'}(\boldsymbol{k}') C_s(\boldsymbol{k}) \times \sum_{\boldsymbol{R}_s, \boldsymbol{R}_{s'}} \times \exp(-\mathrm{i}\boldsymbol{k}' \cdot \boldsymbol{R}_{s'} + i\boldsymbol{k} \cdot \boldsymbol{R}_s) \langle \phi(\boldsymbol{R}_{s'}) | V | \phi(\boldsymbol{R}_s) \rangle. \tag{6}$$

Here we consider only interactions between nearest-neighbor carbon atom sites

$$\langle \phi(\boldsymbol{R}_s) | V | \phi(\boldsymbol{R}_{s'}) \rangle = \begin{cases} \gamma_0 & s, s' (\text{nearest neighbor}) \\ 0 & \text{otherwise.} \end{cases} \tag{7}$$

For a k vector around the K point, we have two possibilities, that is, an intravalley or intervalley scattering process. The D-band corresponds to intervalley scattering. Here we only consider the scattering at the armchair edge [16]. After some calculation, the intervalley $M_{\boldsymbol{k}'\boldsymbol{k}}$ are given by

$$\begin{aligned} M_{\boldsymbol{k}'\boldsymbol{k}} = -\frac{a\gamma_0}{2L_a w(\boldsymbol{k})} \delta(k_x, k'_x) \Bigg[& 2w^2(\boldsymbol{k}) \cos\left\{\frac{(k'_y - k_y)L_a}{2}\right\} \\ & - \left\{ \exp\left(-\mathrm{i}\frac{\sqrt{3}k_x a}{2}\right) + 2\cos\left(\frac{k_y a}{2}\right) \right\} \\ & \times \cos\left\{\frac{k_y a}{2} - \frac{(k'_y - k_y)L_a}{2}\right\} - \left\{ \exp\left(\mathrm{i}\frac{\sqrt{3}k'_x a}{2}\right) \right. \\ & \left. + 2\cos\left(\frac{k'_y a}{2}\right) \right\} \times \cos\left\{\frac{k'_y a}{2} + \frac{(k'_y - k_y)L_a}{2}\right\} \Bigg], \end{aligned} \tag{8}$$

where $\delta(k_x, k'_x)$ is a delta-function due to momentum conservation, and $f(\boldsymbol{k})$ and $w(\boldsymbol{k})$ are given by [19]

$$f(\boldsymbol{k}) = \sum_{i=1}^{3} f_i(\boldsymbol{k}) = \sum_{i=1}^{3} \mathrm{e}^{\mathrm{i}\boldsymbol{k}\cdot\boldsymbol{b}_i}, \tag{9}$$

$$w(\boldsymbol{k}) = \sqrt{|f(\boldsymbol{k})|^2}. \tag{10}$$

The momentum conservation $k_x = k'_x$ in Eq. 8 for the armchair edge is also valid for the zigzag edge. This momentum conservation indicates that the allowed elastic scattering q vector must be perpendicular to the k_x-axis. In the case of the zigzag edge, the intervalley scattering q vector should connect K to K (or K' to K') [16]. Thus, the intervalley scattering cannot occur at the zigzag edge. On the other hand, at the armchair edge, both intravalley and intervalley scattering can occur [16].

3.2. Optical matrix elements and electron–phonon matrix elements

The other matrix elements that are needed for the Raman spectra calculation such as optical matrix elements for absorption and emission, and electron-phonon interaction, are the same ones that we used in the Raman intensity for the first order Raman spectra [20]. Since nanographite does not have curvature, we only consider the electron-phonon interaction for π-electrons [20]. For calculating the lattice vibration amplitude, the number of phonons for the various energies can be calculated by using the Bose–Einstein distribution for phonon emission and absorption ($\beta = 1/k_B T$) with $T = 300$ K.

The electronic structure calculation is based on the extended tight binding (ETB) method [21] and the phonon energy dispersion is calculated by a molecular dynamics calculation in which we adopt Dubay's force constants [22] up to the twentieth nearest neighbors. The calculated phonon dispersion reproduces well the phonon dispersion of graphite obtained by the inelastic X-ray measurements [23]. Further we assume that the iTO phonon branch around K is approximated by the linear function $\omega_q = 1250 + 973q\ \mathrm{cm}^{-1}$ which is discussed in terms of Kohn-anomalies by Piscanec et al. [24]. This approximation for the experimental results is important to reproduce the width and the dispersion of the observed spectra.

4. Calculated results

In Fig. 3 we show the calculated D-band Raman spectra for the three different laser energies of 1.90 (solid), 2.30 (dashed) and 2.70 eV (dotted lines). The D-band peaks in the 1350–1400 cm^{-1} range come from the iTO phonon dispersion branch which has an A_1 symmetry at the K point for which $q = 2k$. The slope of the D-band frequency from the results of Fig. 3 is $\partial\omega_D/\partial E_{laser} = 52\ \mathrm{cm}^{-1}/\mathrm{eV}$, which reproduces the experimental value well.

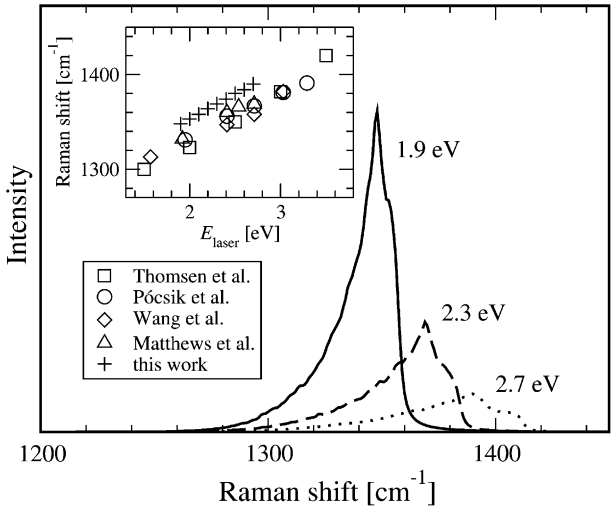

Fig. 3. The calculated Raman spectra of the D-band for $E_{laser} = 1.90$ (solid line), 2.30 (dashed line), 2.70 eV (dotted line) at $L_a = 570$ Å. The inset of the figure is a comparison with the other works [12].

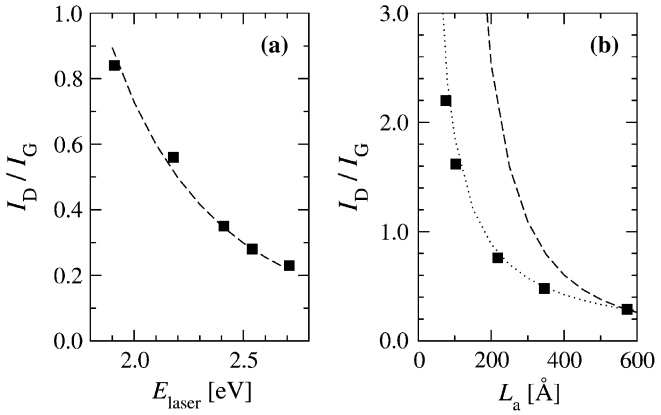

Fig. 4. (a) The laser energy dependence of I_D/I_G at $L_a = 570$ Å. (b) The crystallite size dependence of I_D/I_G at $E_{laser} = 2.41$ eV. The square points and dashed lines are, respectively, experimental and calculated results. The dotted line in Fig. 4b is a calculated result with additional L_a dependence for γ (see detail in text).

Fig. 4 shows the calculated dependence of the I_D/I_G ratio on (a) E_{laser} and (b) L_a (dashed lines). Here we assume that I_G does not depend on either E_{laser} or L_a and that I_G is selected to be a constant. The value of I_G is fitted so as to fit the I_D/I_G value for $L_a = 570$ Å and $E_{laser} = 2.41$ eV. Square points are the experimental data shown for comparison. Both calculated and experimental results give I_D/I_G proportional to E_{laser}^{-4}. It is seen that the E_{laser} dependence of I_D/I_G shows good agreement between theory and experiment, while the L_a dependence shows some discrepancy. Figure 5 shows a log–log plot of the calculated results of the dependence of the I_D/I_G ratio as a function of : (a) E_{laser}, (b) L_a and (c) $L_a^{-2}E_{laser}^{-4}$. The experimental results show that I_D/I_G is proportional to L_a^{-1}, while the calculated results give I_D/I_G proportional to L_a^{-2}. The reason for $I_D/I_G \propto L_a^{-2}$ is the normalization factor L_a^{-1} in Eq. 8. The weak L_a dependence in the experiment might come from: (1) another origin of defects or (2) an L_a dependence

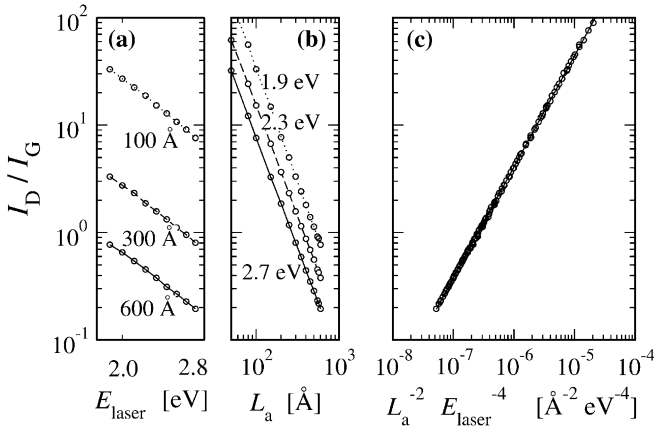

Fig. 5. The log–log plot of the calculated dependence of the ratio I_D/I_G on: (a) the laser energy. (b) the crystallite size L_a. (c) the product $L_a^{-2}E_{laser}^{-4}$ to give a universal curve. Open circles denote calculated values.

on the resonance γ, which will be clarified in future experiments. In fact when we make $\gamma \sim C/\sqrt{L_a}$ (C : constant) for only the elastic scattering process, we can reproduce the experimental results (dotted line in Fig. 4b). The justification for $\gamma \sim C/\sqrt{L_a}$ comes from the fact that (1) carriers move diffusively : $L_a \sim Dt^2$ (D : diffusion constant, t: diffusion time) and (2) from (1) $\gamma \sim \hbar/t \sim \sqrt{D}/\sqrt{L_a}$.

5. Summary

In summary, we have studied the D-band intensity systematically for nanographite materials with different laser excitation energies and crystalline sizes. Using the elastic scattering matrix element that is developed for armchair edges, we can reproduce the excitation energy dependence of the D-band intensity by the double resonance Raman scattering approach. On the other hand, there is some discrepancy for the L_a dependence of the Raman intensity. We need to further investigate the origin of the L_a dependence from both experimental and theoretical standpoints, which will be studied in the near future.

Acknowledgements

The TU authors acknowledge Dr. T. Nakanishi for useful discussions and a Grant-in-Aid (No. 16076201) from MEXT, Japan; we also thank Professor M. Endo for providing us with the heat-treated PPP samples. The UFMG authors acknowledge JST for the support for their travel to Sendai and they also acknowledge support from PRPq-UFMG, FAPEMIG and CNPq, Brazil. The MIT authors acknowledge support under NSF Grants DMR 04-05538.

References

[1] F. Tuinstra, J.L. Koenig, J. Chem. Phys. 53 (1970) 1126.
[2] R.P. Vidano, D.B. Fishbach, L.J. Willis, T.M. Loehr, Solid State Commun. 39 (1981) 341.
[3] Y. Wang, D.C. Aolsmeyer, R.L. McCreery, Chem. Mater. 2 (1990) 557.
[4] T.P. Mernagh, R.P. Cooney, R.A. Johnson, Carbon 22 (1984) 39.
[5] M. Ramsteiner, J. Wagner, Appl. Phys. Lett. 51 (1987) 1355.
[6] M.J. Matthews, M.A. Pimenta, G. Dresselhaus, M.S. Dresselhaus, M. Endo, Phys. Rev. B 59 (1999) R6585.
[7] J. Kastner, T. Pichler, H. Kuzmany, S. Curran, W. Blau, D.N. Weldon, M. Dlamesiere, S. Draper, H. Zandbergen, Chem. Phys. Lett. 221 (1994) 53.
[8] I. Pócsik, M. Hundhausen, M. Koós, L. Ley, J. Non-Cryst. Solids 227–230 (1998) 1083.
[9] PingHeng Tan, S. Dimovski, Y. Gogotsi, Phil. Trans. R. Soc. A 362 (2004) 2289.
[10] E.B. Barros, N.S. Demir, A.G. Souza Filho, J. Mendes Filho, A. Jorio, G. Dresselhaus, M.S. Dresselhaus, Phys. Rev. B 71 (2005) 165422.
[11] A.V. Baranov, A.N. Bekhterev, Y.S. Bobovich, V.I. Petrov, Opt. Spectrosk. 62 (1987) 1036, 612.
[12] C. Thomsen, S. Reich, Phys. Rev. Lett. 85 (2000) 5214.
[13] R. Saito, A. Jorio, A.G. Souza Filho, G. Dresselhaus, M.S. Dresselhaus, M.A. Pimenta, Phys. Rev. Lett. 88 (2002) 027401.
[14] M. Endo, C. Kim, T. Hiraoka, T. Karasaki, K. Nishimura, M.J. Matthews, S.D.M. Brown, M.S. Dresselhaus, J. Mater. Res. 13 (1998) 2023.
[15] L.G. Cançado, K. Takai, T. Enoki, M. Endo, Y.A. Kim, H. Mizusaki, A. Jorio, L.N. Coelho, R. Magalhães-Paniago, M.A. Pimenta, Appl. Phys. Lett. 88 (2006) 163106.
[16] L.G. Cançado, M.A. Pimenta, B.R.A. Neves, M.S.S. Dantas, A. Jorio, Phys. Rev. Lett. 93 (2004) 247401.
[17] K. Nakada, M. Fujita, G. Dresselhaus, M.S. Dresselhaus, Phys. Rev. B 54 (1996) 17954.
[18] M.S. Dresselhaus, G. Dresselhaus, R. Saito, A. Jorio, Phys. Rep. 409 (2005) 47.
[19] R. Saito, G. Dresselhaus, M.S. Dresselhaus, Physical Properties of Carbon Nanotubes, Imperial College Press., London, 1998.
[20] J. Jiang, R. Saito, A. Grüneis, S.G. Chou, Ge. G. Samsonidze, A. Jorio, G. Dresselhaus, M.S. Dresselhaus, Phys. Rev. B 71 (2005) 205420.
[21] Ge. G. Samsonidze, R. Saito, N. Kobayashi, A. Grüneis, J. Jiang, A. Jorio, S.G. Chou, G. Dresselhaus, M.S. Dresselhaus, Appl. Phys. Lett. 85 (2004) 5703.
[22] O. Dubay, G. Kresse, H. Kuzmany, Phys. Rev. Lett. 88 (2002) 235506.
[23] J. Maultzsch, S. Reich, C. Thomsen, H. Requardt, P. Ordejon, Phys. Rev. Lett. 92 (2004) 075501.
[24] S. Piscanec, M. Lazzeri, M. Mauri, A.C. Ferrari, J. Robertson, Phys. Rev. Lett. 93 (2004) 185503.